

## Early *in vivo* assessment of angiostatic therapy efficacy by molecular MRI

Willem J. M. Mulder,<sup>\*,1</sup> Daisy W. J. van der Schaft,<sup>†</sup> Petra A. I. Hautvast,<sup>†</sup> Gustav J. Strijkers,<sup>\*</sup> Gerben A. Koning,<sup>‡</sup> Gert Storm,<sup>§</sup> Kevin H. Mayo,<sup>||</sup> Arjan W. Griffioen,<sup>†</sup> and Klaas Nicolay<sup>\*</sup>

<sup>\*</sup>Biomedical NMR, Department of Biomedical Engineering, Eindhoven University of Technology, Eindhoven, The Netherlands; <sup>†</sup>Angiogenesis Laboratory, Research Institute for Growth and Development, Department of Pathology/Internal Medicine, Maastricht University and University Hospital, Maastricht, The Netherlands; <sup>‡</sup>Department of Radiation, Radioisotopes, and Reactors, Faculty of Applied Sciences, Delft University of Technology, Delft, The Netherlands; <sup>§</sup>Department of Pharmaceutics, Utrecht Institute for Pharmaceutical Sciences, Utrecht, The Netherlands; and <sup>||</sup>Department of Biochemistry, Molecular Biology and Biophysics, University of Minnesota, Minneapolis, Minnesota, USA

**ABSTRACT** Noninvasive diagnostic imaging methods to establish the efficacy of angiostatic therapies are becoming increasingly important with the first Food and Drug Administration approvals of such agents. Magnetic resonance molecular imaging is an imaging technique that allows the visualization of pathological processes *in vivo* with a better spatial resolution as compared with nuclear methods, such as photon emission tomography and single photon emission computed tomography. In this study, we used  $\alpha v\beta 3$  targeted bimodal liposomes to quantitate angiogenesis in a tumor mouse model with magnetic resonance imaging (MRI) and to evaluate the therapeutic efficacy of the angiogenesis inhibitors anginex and endostatin. The MRI findings were validated with fluorescence microscopy and showed a very good correlation with the microvessel density. In conclusion, this study provides evidence that molecular MRI can be used to noninvasively measure the efficacy of angiogenesis inhibitors during the course of therapy.—Mulder, W. J. M., van der Schaft, D. W. J., Hautvast, P. A. I., Strijkers, G. J., Storm, G., Mayo, K. H., Griffioen, A. W., Nicolay, K. Early *in vivo* assessment of angiostatic therapy efficacy by molecular MRI. *FASEB J.* 21, 000–000 (2007)

**Key Words:** molecular imaging • tumor angiogenesis •  $\alpha v\beta 3$ -integrin

THERAPEUTIC INTERVENTIONS TO REDUCE tumor growth by inhibition of angiogenesis, the formation of new blood vessels, have rapidly evolved since it was hypothesized that tumor growth and metastasis are angiogenesis dependent (1). Extensive research and clinical trials have resulted in the Food and Drug Administration approval of the first antiangiogenic agent in 2004 (2). The innovation of this approach is that angiogenesis inhibitors target cells that support tumor growth, *i.e.*, endothelial cells, which are directly accessible from the bloodstream (3, 4). There are several classes of angiogenesis inhibitors, *e.g.*, growth

factor blockers (5), inhibitors of growth factor signaling (6), modulators of extracellular matrix (7), and direct inhibitors of endothelial cell proliferation or migration (8–10). Increasing numbers of these inhibitors are currently being tested in clinical trials.

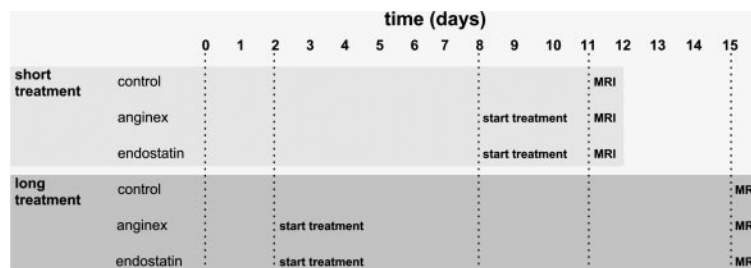
With these developments, it is also increasingly important to assess the efficacy of these agents, preferably in a noninvasive way. Different methods are developed to monitor angiogenic activity during the course of treatment. Preclinically, the effects of angiostatic drugs are commonly evaluated in mouse models by studying the microvessel density (MVD) and tumor growth and also by the determination of circulating levels of angiogenic factors, such as vascular endothelial growth factor or basic fibroblast growth factor or serum levels of other molecules. With the use of these procedures, however, the therapeutic effect on tumor growth can only be seen after a certain time of treatment. Also, when agents that directly target angiogenically activated endothelial cells are used, measurement of angiogenic factors that are released by the tumor cells in the serum may not be the ideal approach. The optimal measurement of angiogenesis *in vivo* to quickly evaluate the therapeutic response of the tumor still has to be established.

In mouse models, for example, many angiogenesis inhibitors, like anginex and endostatin, have shown to decrease the MVD (8, 11) in the tumor tissue and therefore this parameter may be used to predict therapeutic effect.

A disadvantage of MVD is that it can only be determined using an invasive procedure followed by staining for endothelial markers in histological sections of excised material. Therefore, an alternative noninvasive method that correlates with the vessel density in the

<sup>1</sup> Correspondence: Biomedical NMR, Eindhoven University of Technology, PO Box 513, 5600 MB Eindhoven, The Netherlands. E-mail: w.j.m.mulder@tue.nl  
doi: 10.1096/fj.06-6791com

**Figure 1.** Schematic representation of experimental setup. At day 0, mice were inoculated with melanoma B16F10 cells. All groups consisted of 4 or 5 animals.



tumor would be highly beneficial, since methods to determine and visualize the MVD *in vivo* would allow longitudinal monitoring and thus facilitate the evaluation of a given antiangiogenic therapy.

Magnetic resonance (MR) imaging (MRI) is a powerful noninvasive imaging method capable of generating high resolution images of soft tissues, such as tumors. Hemodynamic parameters such as vascular permeability, perfusion, and plasma volume can be visualized with dynamic contrast enhanced (DCE) MRI, and these have been demonstrated to correlate with MVD (12). Furthermore, recent developments in the field of molecular imaging (13, 14) in which the aim is to visualize pathological processes at the molecular level, *e.g.*, by targeting contrast material to endothelial cell surface receptors that are up-regulated as a consequence of the pathology, broaden the use of MRI to the identification of molecular markers. This greatly enhances the utility of this imaging method in the field of tumor angiogenesis. Powerful MR contrast agents that specifically associate with activated blood vessels would allow a direct visualization of the angiogenesis activity in the tumor. We recently developed a liposomal contrast agent that can be used for molecular imaging of tumor angiogenesis activity (15). This agent was shown to exhibit excellent fluorescent and paramagnetic properties (16). The liposomes are roughly 150 nm in size and are typically conjugated with 700 cyclic RGD peptides per particle. This contrast agent has been shown to enable MRI-based molecular imaging of the activated endothelium in tumor bearing mice by targeting the  $\alpha\beta 3$ -integrin (15), an angiogenesis specific marker up-regulated on activated endothelial cells (3).

In the present study, we have used the above contrast agent in combination with *in vivo* MRI and *ex vivo* fluorescence microscopy to image ongoing angiogenesis for evaluating the effects of angiogenesis inhibitors at two different time points. The method described provides a tool to noninvasively image angiogenic endothelium *in vivo* as well as to monitor the effects of angiostatic therapy.

## MATERIALS AND METHODS

The animal experiments were approved by the local ethical review committee. At day 0, 30 6-wk-old C57BL/6 mice (Charles River, Maastricht, The Netherlands) were inoculated with  $1 \times 10^5$  B16F10 cells (provided by Dr J. Fidler, Houston, TX, USA) subcutaneously on the right flank. For

the 2 week treatment schedule, an Alzet osmotic minipump (Charles River, Maastricht, The Netherlands) was placed subcutaneously 2 days after the inoculation. For the 3 day treatment, the minipumps were placed at day 8. The minipumps were surgically implanted as described previously (11). In short, the mice were anesthetized with ketamin/xylazine. A small incision was made in the skin on the back of the mouse; the skin was opened using a blunt scissor; and the minipump was put underneath the skin. The skin was subsequently closed with sutures. The minipumps administered either endostatin (4 mg/kg/day, EntreMed, Rockville, MD, USA), anginex (8 mg/kg/day, synthesized as described previously in ref 10), or physiological salt. Between day 6 and 9, the tumors became visible in all mice, and tumor volume was measured daily. Tumor volumes were calculated as follows:  $\text{width}^2 \times \text{length} \times 0.52$  (in  $\text{mm}^3$ ). The treatment protocol is depicted in Fig. 1. For the short-treated animals, the control group and the endostatin-treated group consisted of five mice, and the anginex treated group of five mice. For the long-treated animals, the control group consisted of four mice, and both the anginex and endostatin-treated groups of five mice.

## MRI experiments

Pegylated and paramagnetic RGD liposomes were prepared by lipid film hydration as described previously (15, 16). All the MRI experiments were performed on a 6.3 Tesla horizontal bore magnet (Oxford Instruments, Oxon, England) interfaced to a Bruker Biospec (Bruker, Ettlingen, Germany) MRI console. A 3 cm quadrature-driven birdcage coil was used.

Mice were anesthetized with isoflurane (1.5–2%) and placed in a home built cradle, equipped with a mask for anesthesia gas supply and a warm water pad. An infusion line with RGD liposomes was placed and fixed in the tail vein to inject the contrast agent during the MRI experiment. The injection dose was 100  $\mu\text{l}$  of a 40 mM liposomal suspension. Respiration was monitored with a balloon sensor connected to an ECG/respiratory unit (Rapid Biomedical, Würzburg, Germany).

First, multislice  $T_2$ -weighted (TR=2000 ms, TE=30 ms, matrix size  $128 \times 128$ , slice thickness 1 mm, NEX=2, FOV= $3 \times 3 \text{ cm}^2$ ) images were acquired to localize the tumor. Next,  $T_1$ -weighted images (TR=800 ms, TE=9 ms, matrix size  $128 \times 128$ , slice thickness 1 mm, NEX=16, FOV= $3 \times 3 \text{ cm}^2$ ) from 21 consecutive slices were generated before the contrast agent was injected. Forty-five minutes after the contrast agent was injected,  $T_1$ -weighted images were acquired with the same parameters as described above.

## MRI Analysis

The tumors were segmented by manually drawing a region of interest (ROI) around the tumor area for all slices in the  $T_2$ -weighted images. The pixel intensities in the tumor ROIs after injection of the contrast agents were compared with the

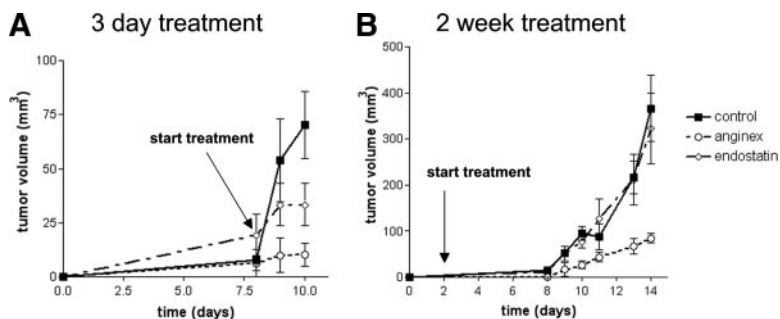


**Figure 2.** Tumor growth profiles of short-term treatment group (A) and long-term treatment group (B). Animals were treated with endostatin (4 mg/kg/day) or anginex (8 mg/kg/day) using osmotic minipumps. Saline-treated animals served as controls.

precontrast intensities. A pixel was considered significantly enhanced when its intensity was increased by at least five times the mean noise level. The number of enhanced pixels in the tumors, in terms of percentage of the total tumor area, was averaged for the different groups. All averages are reported as mean  $\pm$  SE. Statistical comparison of the means was performed using Student's *t* tests.  $P < 0.05$  was considered statistically significant.

### Fluorescence microscopy of tumor sections

Tumors were dissected from the animals, frozen in isopentane, and stored at  $-80^{\circ}\text{C}$  until analysis.  $4\ \mu\text{m}$  sections were cut, air-dried, fixed in acetone at  $-20^{\circ}\text{C}$  for 20 min, air-dried again, rinsed in PBS, and blocked in 5% BSA and 5% normal mouse serum in PBS for 30 min. The slides were mounted with Immumount (BD Biosciences, San Jose, CA) containing  $1\ \mu\text{g}/\text{ml}$  4',6'-diam idino-2-phenylidole (DAPI; Sigma-Aldrich, Zwijndrecht, The Netherlands) for nuclear counterstaining. For visualization of all blood vessels, sections were stained indirectly with monoclonal rat anti-CD31 antibody (Ab; Pharmingen, BD Biosciences, Alphen aan den Rijn, the Netherlands) and polyclonal goat antirat Ig Ab labeled with FITC (PICKCELL, Amsterdam, the Netherlands). Rhodamine from the RGD liposomes, DAPI, and FITC fluorescence were simultaneously imaged using a fluorescence microscope (Leica DM550B, a Leica DC300FX camera, and Leica QWinV3 software, Wetzlar, Germany).

### Microvessel density assessment

Cryosections ( $4\ \mu\text{m}$ ) were put on organosilane-coated object slides, air-dried for 24 h at room temperature, and fixed with acetone at  $-20^{\circ}\text{C}$  for 20 min (Sigma). Endogenous peroxidase was blocked by incubation in 0.3%  $\text{H}_2\text{O}_2$  in methanol for 30 min. Sections were blocked for nonspecific Ab binding with 5% BSA and 5% mouse serum in PBS. The slides were incubated with anti-mouse CD31 Ab (Pharmingen) for 1 h. After incubation with horse radish peroxidase labeled anti-rat Ab (Vector Laboratories, Burlingame, CA, USA) for 30 min, the slides were developed with diaminobenzidine (Sigma) and counterstained with hematoxylin (Merck) and mounted in Entellan (Merck, Darmstadt, Germany). The MVD was evaluated as described previously (11). In short, two independent observers assessed MVD by counting of vessels at 200 times magnification in 5 random tumor areas of  $0.25\ \text{mm}^2$  for each tumor. Significance of observed differences was assessed using Student's *t* tests.

## RESULTS

### Treatment effects on tumor growth

B16F10 mouse melanoma tumors were grown on the flank of C57BL6 mice and treated with endostatin (4

mg/kg/day) or anginex (8 mg/kg/day). Both antiangiogenesis agents were administered by continuous subcutaneous infusion, using osmotic minipumps, according to the schedule shown in Fig. 1. In the first group of animals, the treatment was initiated 8 days after the melanoma cells were inoculated and after established tumors were visible. The treatment lasted 3 days and resulted in a significant inhibition of the tumor growth for both endostatin and anginex (Fig. 2A). The second group of animals that were treated for 2 wk was implanted with osmotic minipumps 2 days after inoculation with melanoma cells. At the end of the treatment period, anginex significantly inhibited tumor growth by 60%, as compared with control mice. The tumor growth profile of endostatin at the concentration used, in contrast to the situation after 3 days, did not significantly differ from that of the control animals (Fig. 2B), although tumor growth inhibition was expected from previous studies (8).

### *In vivo* MRI and fluorescence microscopy on administration of RGD liposomes

*In vivo* MRI experiments with RGD liposomes were carried out on anesthetized mice. After localization of the tumor with a  $T_2$ -weighted scan,  $T_1$ -weighted MR scans were acquired before (Fig. 3A) and 45 min after liposomes were intravenously injected (Fig. 3B). The total scan time per animal was 2 h. As determined from the increase in MR signal intensity, the contrast agent accumulated in the tumor. MR signal was most pronounced at the rim of the tumor. In Fig. 3C, imaging voxels that had a significantly increased signal intensity are color coded. The relative amount of enhanced voxels expressed as the percentage of the total tumor area was calculated from the MRI slices covering the entire tumor for all animals.

After the MR experiments, the mice were killed and tumors were dissected, frozen, and sectioned. The sections were hematoxylin and eosin stained and counterstained with DAPI to visualize the individual tumor cell nuclei. Blood vessels were immunohistochemically stained by using the endothelial cell specific CD31 Ab conjugated to FITC. Fluorescence microscopy revealed the exclusive association of RGD liposomes with tumor blood vessels (Fig. 4) for control tumors (Fig. 4A) as well as for treated tumors (Fig. 4B, C).

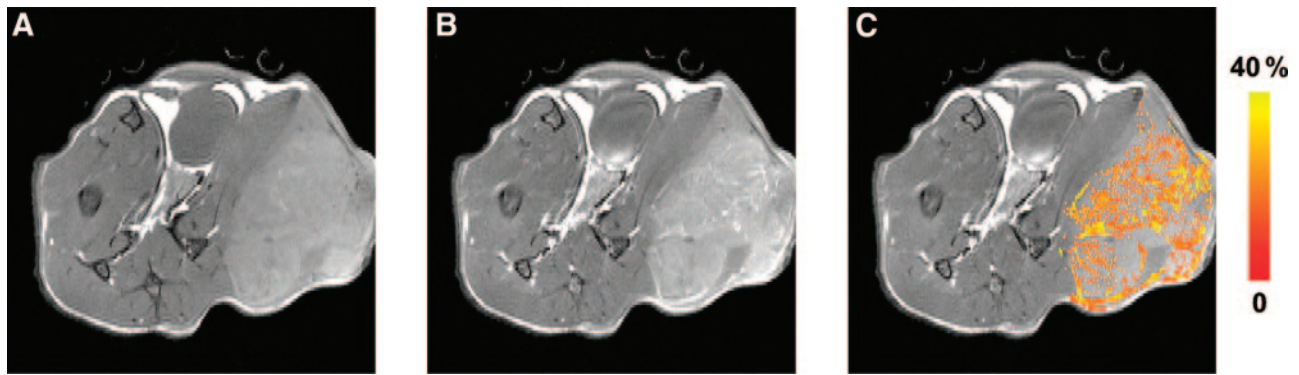


**Figure 3.** A typical example of an MR image through tumor of an animal before (A) and after (B) injection with paramagnetic RGD liposomes. Pixels in tumor with signal enhancement of at least 5 times the noise level were color coded (C). From these data, percentage of tumor area with significant enhancement was determined.

### Comparison of *ex vivo* MVD determinations and *in vivo* MRI data

In the short-term treatment groups, the MVD of the endostatin-treated group was significantly reduced as compared with the control group (Fig. 5A, left). The anginex group had a MVD that did not significantly differ from the control group. The MVDs for the long-term treatment groups revealed a different pattern. Anginex-treated animals had a significantly reduced MVD, whereas the endostatin-treated group had a slightly higher but not significantly different MVD compared with the control animals. These latter observations correspond with the tumor growth suppression profiles (Fig. 2B). For the endostatin group, no inhibition of tumor growth was observed, whereas anginex-treated animals did show considerable growth inhibition when treated for a longer time period.

MRI data sets from all animals were analyzed by determining the percentage of significantly enhanced voxels within a tumor. In Fig. 5B, the results of the analysis are depicted. A similar trend was found as for the MVD determinations (Fig. 5A). For the short-term

treatment group, only the animals that were given endostatin had a significantly reduced percentage of the tumor with contrast enhancement compared with the control group, whereas for the long-term treated animals only the anginex group showed a significantly reduced tumor enhancement on MRI. The slightly lower, albeit nonsignificant, percentage of tumor enhancement of the endostatin-treated animals did not correspond to the response as seen for the MVD value in this group. Nevertheless, when the MVD and MRI data were normalized to the corresponding values in control animals, overall the trend found by *in vivo* molecular MRI of tumor angiogenesis closely reflected the treatment effects as deduced from *ex vivo* MVD quantification for both the short-term treatment group (Fig. 5C) and the long-term treatment group (Fig. 5D).

### DISCUSSION

Imaging methods to visualize molecular details of biological processes are rapidly being developed and hold great promise for earlier screening and improved diag-

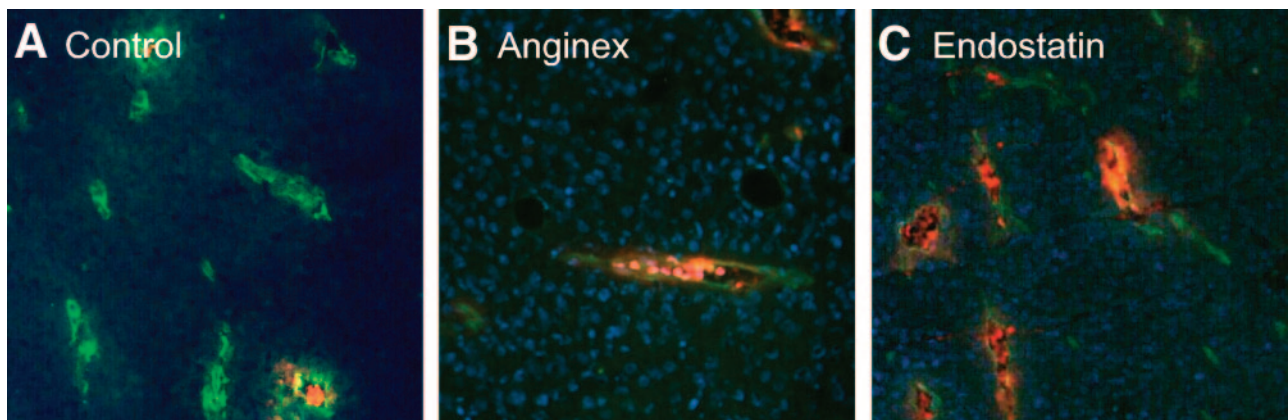


**Figure 4.** Fluorescence microscopy of DAPI-stained 4  $\mu\text{m}$  sections from dissected tumors revealed exclusive association of RGD liposomes with blood vessels, both for control animals (A) and treated animals (B, C). Vessel staining was done with an endothelial cell specific anti-CD31 Ab. Red fluorescence represents RGD liposomes, and green fluorescence represents blood vessels (FITC).

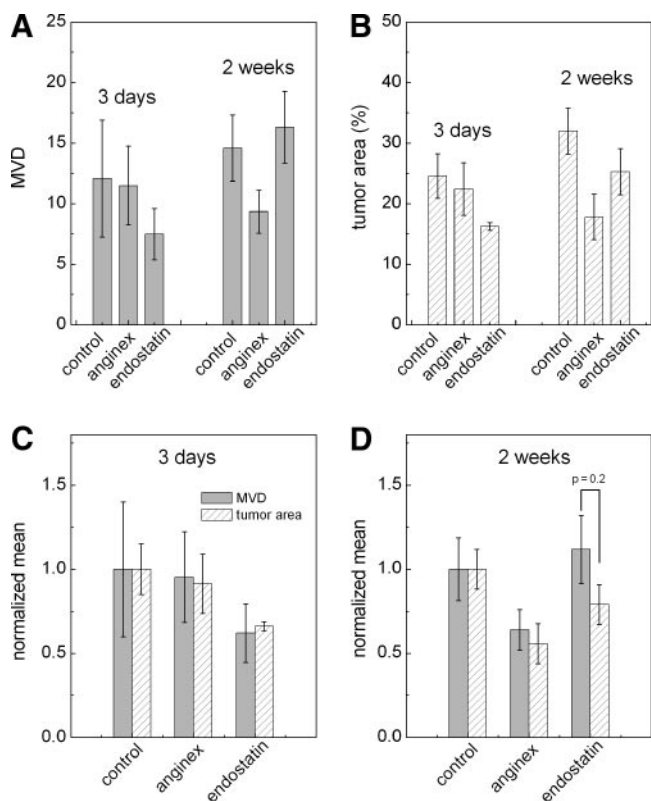


**Figure 5.** A) Quantification of MVD as mean number of vessels per  $0.25 \text{ mm}^2$ . B) Percentage of tumor with significant MRI signal enhancement after iv injection with RGD liposomes. C, D) Comparison of normalized MVD and tumor area for short-term treatment group (C) and long-term treatment group (D).

nosis of diseases (13, 14). Traditionally, such as sensitive techniques like such as photon emission tomography (PET) and single photon emission computed tomography (SPECT) are the domain of molecular imaging in the clinical setting. Molecules with target specificity, like antibodies and peptides, are conjugated with a radiolabel to visualize receptor binding using these nuclear techniques. The poor anatomical definition and resolution of PET and SPECT, however, pose a limit to their ability to localize receptor expression. Diagnostic imaging methods with a good spatial resolution and anatomical contrast, like computed tomography and MRI, are not ideal for molecular imaging purposes, because of their low inherent sensitivity. Nevertheless, with the development of potent nanoparticulate and paramagnetic contrast agents, MRI is becoming suitable for molecular receptor imaging, especially for vascular targets. Most studies that report on the use of molecular MRI are so-called proof-of-concept studies that demonstrate the applicability of MRI as a molecular imaging modality. An early study of this kind was performed by Sipkins *et al.* (17), who demonstrated the detection of angiogenesis with MRI using polymerized paramagnetic vesicles conjugated with antibodies specific for  $\alpha v \beta 3$ -integrin. Paramagnetic perfluorocarbon microemulsions targeted to the same receptor

have been applied to visualize angiogenesis in rabbit models of atherosclerosis (18) and cancer (19).

Studies that report on the application of molecular MRI to visualize transgene expression or the effects of therapeutic interventions are limited. Iron oxide nanoparticles conjugated with transferrin specific antibodies have been used to visualize transgene expression in mice inoculated with tumor cells on one flank and transgenic tumor cells over-expressing the transferrin receptor on the other flank (20). The C2 domain of synaptotagmin I conjugated to iron oxide nanoparticles has been used to visualize apoptosis induced by a chemotherapeutic agent (21).

Although the above studies demonstrated the feasibility of using MRI for molecular imaging purposes, extending the utility of such targeted contrast agents may be realized by also equipping the agent with optical properties. Fluorescent as well as paramagnetic albumin for example has been demonstrated to be valuable for visualizing and quantifying angiogenesis and lymphatic drain with both MRI and fluorescence microscopy (22). In a previous study (15), we reported on a method to directly target and visualize activated tumor vessels with *in vivo* MRI by using  $\alpha v \beta 3$  targeted bimodal liposomes and demonstrated the exclusive and specific binding of the contrast agent to these vessels by *ex vivo* fluorescence microscopy.

In the present study, we applied this technology to evaluate the early effects of angiogenesis inhibitors. As indicated in the Introduction, common methods to assess the therapeutic efficacy of angiostatic agents are by determining circulating growth factors, tumor growth, and the MVD. Several indirect noninvasive imaging methods, such as DCE MRI (12) and PET (23), have been developed to provide information on the MVD *in vivo*. A major drawback of both these techniques is that an indirect parameter for the MVD, namely the vessel permeability or methionine uptake, is determined. A second drawback of PET is its poor spatial resolution. The direct visualization of angiogenic blood vessels in a tumor can be realized by using bimodal liposomes targeted to the  $\alpha v \beta 3$ -integrin. This may be a better measure for angiogenesis than the previous methods. Indeed, the molecular MRI technique, as presented here, shows a good correlation with the MVD as quantified *ex vivo* with immunohistochemical analysis. In case the MVD and the data obtained by the molecular MRI technique of treated animals were normalized to the values of the control groups, a direct comparison of both parameters was possible, which revealed a high correlation. Furthermore, given that the MVD correlates with therapeutic efficacy (8, 11), the MRI technique may also provide a way to noninvasively and longitudinally evaluate effects of angiogenesis inhibitors. In addition, since the MVD is a useful prognostic indicator in the clinical setting, it is valuable to explore the utility of the present technology as a surrogate marker of treatment outcome, without the need for analysis of biopsy material.

Next to cancer, other pathological processes are also

associated with angiogenesis. In atherosclerosis, for example, the network of microvessels in the wall of larger arteries (vasa vasorum) expands through angiogenesis (24). Rheumatoid arthritis is a pathological process that results in the destruction of cartilage and bone by proliferative synovitis. This is characterized by infiltration of inflammatory cells and formation of new blood vessels, which occurs already in the early stage of the disease and supports progression of the arthritis (25). The MVD therefore may also be an indicator for the stage and severity of these disorders. It has been shown that these diseases could also benefit from antiangiogenic therapy, which could be monitored by our MRI-based method.

Other and potentially more specific markers of angiogenesis may also be targeted using the same contrast agent when conjugated to a different ligand that targets angiogenic endothelium. Furthermore, the depiction the severity of inflammatory processes related to pathologies like atherosclerosis, arthritis, multiple sclerosis, or after ischemia may be realized by linking ligands specific for endothelial cell adhesion molecules.

In conclusion, a methodology was presented that allows the rapid evaluation of the efficacy of angiostatic therapy by quantifying angiogenesis with molecular MRI *in vivo*. The MRI findings show a very good correlation with angiogenesis, as assessed by *ex vivo* MVD determination. Therefore, molecular MRI by targeting the  $\alpha v \beta 3$ -integrin, as presented in this study, may be used to stage the disease, to facilitate treatment planning, and to more accurately and quickly predict therapeutic response. FJ

This study was funded in part by the EC-FP6-project DiMI, LSHB-CT-2005-512146, and by the BSIK program entitled Molecular Imaging of Ischemic Heart Disease (project number BSIK03033).

## REFERENCES

1. Abdollahi, A., Hlatky, L., and Huber, P. E. (2005) Endostatin: the logic of antiangiogenic therapy. *Drug. Resist. Updat.* **8**, 59–74
2. Folkman, J. (2004) Endogenous angiogenesis inhibitors. *APMIS* **112**, 496–507
3. Griffioen, A. W. and Molema, G. (2000) Angiogenesis: potentials for pharmacologic intervention in the treatment of cancer, cardiovascular diseases, and chronic inflammation. *Pharmacol. Rev.* **52**, 237–268
4. Kerbel, R. and Folkman, J. (2002) Clinical translation of angiogenesis inhibitors. *Nat. Rev. Cancer.* **2**, 727–739
5. Kim, K. J., Li, B., Winer, J., Armanini, M., Gillett, N., Phillips, H. S. and Ferrara, N. (1993) Inhibition of vascular endothelial growth factor-induced angiogenesis suppresses tumour growth in vivo. *Nature* **362**, 841–844
6. Matthews, K. (2006) Use of SU11248 to inhibit proangiogenic growth factors in renal-cell carcinoma patients *Nat. Clin. Pract. Oncol.* **3**, 119
7. Beliveau, R., Gingras, D., Kruger, E. A., Lamy, S., Sirois, P., Simard, B., Sirois, M. G., Tranqui, L., Baffert, F., Beaulieu, E. *et al.* (2002) The antiangiogenic agent neovastat (AE-941) inhibits vascular endothelial growth factor-mediated biological effects. *Clin. Cancer Res.* **8**, 1242–1250
8. O'Reilly, M. S., Boehm, T., Shing, Y., Fukai, N., Vasios, G., Lane, W. S., Flynn, E., Birkhead, J. R., Olsen, B. R. and Folkman, J. (1997) Endostatin: an endogenous inhibitor of angiogenesis and tumor growth. *Cell* **88**, 277–285
9. Benezra, R. and Rafii, S. (2004) Endostatin's endpoints-Deciphering the endostatin antiangiogenic pathway. *Cancer Cell* **5**, 205–206
10. Griffioen, A. W., van der Schaft, D. W., Barendsz-Janson, A. F., Cox, A., Struijker Boudier, H. A., Hillen, H. F. and Mayo, K. H. (2001) Anginex, a designed peptide that inhibits angiogenesis. *Biochem. J.* **354**, 233–242
11. Van der Schaft, D. W., Dings, R. P., de Lussanet, Q. G., van Eijk, L. I., Nap, A. W., Beets-Tan, R. G., Bouma-Ter Steege, J. C., Wagstaff, J., Mayo, K. H. and Griffioen, A. W. (2002) The designer anti-angiogenic peptide anginex targets tumor endothelial cells and inhibits tumor growth in animal models. *FASEB J.* **16**, 1991–1993
12. De Lussanet, Q. G., Beets-Tan, R. G., Backes, W. H., van der Schaft, D. W., van Engelshoven, J. M., Mayo, K. H. and Griffioen, A. W. (2004) Dynamic contrast-enhanced magnetic resonance imaging at 1.5 Tesla with gadopentetate dimeglumine to assess the angiostatic effects of anginex in mice. *Eur. J. Cancer* **40**, 1262–8
13. Weissleder, R. (2002) Scaling down imaging: molecular mapping of cancer in mice. *Nat. Rev. Cancer* **2**, 11–18
14. Weissleder, R. and Mahmood, U. (2001) Molecular imaging. *Radiology* **219**, 316–333
15. Mulder, W. J., Strijkers, G. J., Habets, J. W., Bleeker, E. J., van der Schaft, D. W., Storm, G., Koning, G. A., Griffioen, A. W. and Nicolay, K. (2005) MR molecular imaging and fluorescence microscopy for identification of activated tumor endothelium using a bimodal lipidic nanoparticle. *FASEB J.* **19**, 2008–2010
16. Mulder, W. J., Strijkers, G. J., Griffioen, A. W., van Bloois, L., Molema, G., Storm, G., Koning, G. A., and Nicolay, K. (2004) A liposomal system for contrast-enhanced magnetic resonance imaging of molecular targets. *Bioconjug. Chem.* **15**, 799–806
17. Sipkins, D. A., Cheresesh, D. A., Kazemi, M. R., Nevin, L. M., Bednarski, M. D., and Li, K. C. (1998) Detection of tumor angiogenesis in vivo by alphaVbeta3-targeted magnetic resonance imaging. *Nat. Med.* **4**, 623–626
18. Winter, P. M., Morawski, A. M., Caruthers, S. D., Fuhrhop, R. W., Zhang, H., Williams, T. A., Allen, J. S., Lacy, E. K., Robertson, J. D., Lanza, G. M. *et al.* (2003) Molecular imaging of angiogenesis in early-stage atherosclerosis with alpha(v)beta3-integrin-targeted nanoparticles. *Circulation* **108**, 2270–2274
19. Winter, P. M., Caruthers, S. D., Kassner, A., Harris, T. D., Chinen, L. K., Allen, J. S., Lacy, E. K., Zhang, H., Robertson, J. D., Wickline, S. A. *et al.* (2003) Molecular imaging of angiogenesis in nascent Vx-2 rabbit tumors using a novel alpha(nu)beta3-targeted nanoparticle and 1.5 tesla magnetic resonance imaging. *Cancer Res.* **63**, 5838–5843
20. Weissleder, R., Moore, A., Mahmood, U., Bhorade, R., Benveniste, H., Chiocca, E. A., and Basilion, J. P. (2000) In vivo magnetic resonance imaging of transgene expression. *Nat. Med.* **6**, 351–355
21. Zhao, M., Beaugregard, D. A., Loizou, L., Davletov, B. and Brindle, K. M. (2001) Non-invasive detection of apoptosis using magnetic resonance imaging and a targeted contrast agent. *Nat. Med.* **7**, 1241–1244
22. Dafni, H., Israely, T., Bhujwalla, Z. M., Benjamin, L. E. and Neeman, M. (2002) Overexpression of vascular endothelial growth factor 165 drives peritumor interstitial convection and induces lymphatic drain: magnetic resonance imaging, confocal microscopy, and histological tracking of triple-labeled albumin. *Cancer Res.* **62**, 6731–6737
23. Kracht, L. W., Frieze, M., Herholz, K., Schroeder, R., Bauer, B., Jacobs, A. and Heiss, W. D. (2003) Methyl-[<sup>11</sup>C]-l-methionine uptake as measured by positron emission tomography correlates to microvessel density in patients with glioma. *Eur. J. Nucl. Med. Mol. Imaging* **30**, 868–873
24. Moulton, K. S. (2001) Plaque angiogenesis and atherosclerosis. *Curr. Atheroscler. Rep.* **3**, 225–233
25. Roccaro, A. M., Russo, F., Cirulli, T., Di Pietro, G., Vacca, A. and Dammacco, F. (2005) Antiangiogenesis for rheumatoid arthritis. *Curr. Drug. Targets Inflamm. Allergy* **4**, 27–30

Received for publication July 13, 2006.

Accepted for publication September 22, 2006.